

A GEOSTATISTICAL APPROACH TO MODELING CLIMATE TELECONNECTIONS

BY JOSHUA HEWITT* , JENNIFER A. HOETING* , JAMES DONE[†] AND ERIN TOWLER[†]

Colorado State University and National Center for Atmospheric Research[†]*

Abstract: We propose a geostatistical model to address spatial problems that violate a central tenant of spatial statistics: that distant processes are weakly correlated or independent. The model draws on ideas from spatially varying coefficient models and additionally uses predictive process ideas to overcome modeling challenges in applications. We adopt a hierarchical Bayesian framework to conduct inference and make predictions and use this model to improve predictions of average Winter precipitation in Florida by accounting for teleconnection effects with Pacific Ocean sea surface temperatures. We also discuss physical motivations and interpretations for our model.

1. Introduction. We propose a geostatistical model to address spatial problems that violate a central tenant of spatial statistics: that distant processes are weakly correlated or independent. The flexibility of hierarchical models makes them uniquely suited to address a wide variety of problems in spatial statistics. While most uses of hierarchical models in spatial statistics solve problems that assume distant processes are weakly correlated or independent, not all spatial data are consistent with this tenant.

The climate science term, teleconnection, refers to correlations that global-scale physics create between distant locations. The Pacific Decadal Oscillation (PDO) is a well-known teleconnection in which specific remote covariates—North Pacific sea surface temperatures—impact local climate variables across the United States, including temperature and precipitation. [Mantua et al. \(1997\)](#) introduce the PDO and additionally link its impact to Salmon populations in Alaska, Washington, and Oregon. This motivates the need to consider teleconnection effects in local climate and climate impact analyses. Numerous teleconnections are documented, and several teleconnections can simultaneously impact a single local variable. While the PDO also impacts Florida precipita-

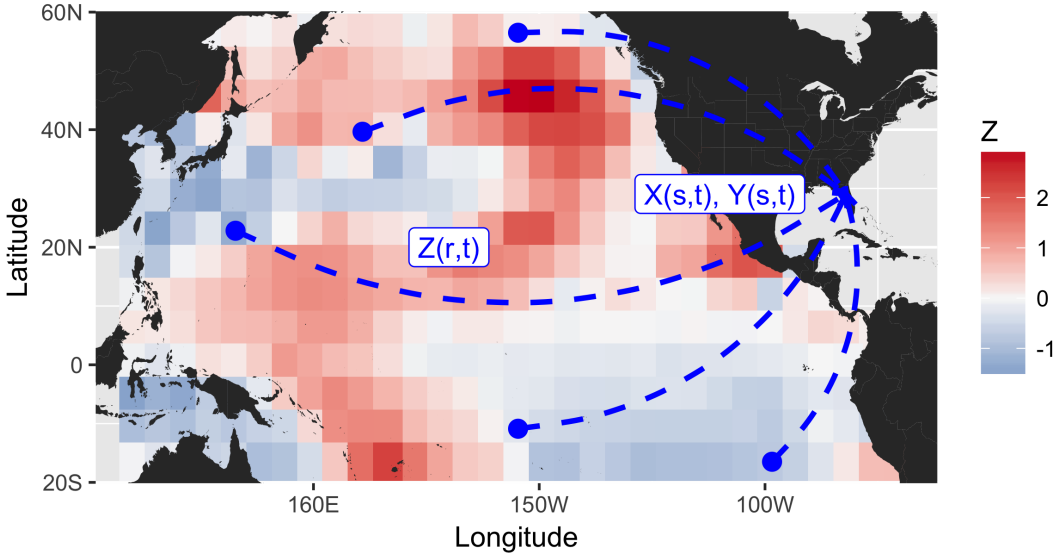


Fig 1: Schematic illustration of a teleconnection problem. Florida precipitation $Y(s, t)$ is influenced by both local covariates $X(s, t)$ and remote covariates $Z(r, t)$. The remote covariates plotted are average monthly Pacific Ocean sea surface temperature standardized anomalies from Winter, 2013. The data come from the ERA-Interim reanalysis dataset (Dee et al., 2011).

tion, Pacific Ocean sea surface temperatures along the equator have a greater impact through the El Niño-Southern Oscillation (ENSO) teleconnection (Douglas and Englehart, 1981; Misra and Di-Napoli, 2013; Ashok et al., 2007; Mantua et al., 1997). Figure 1 schematically illustrates the general teleconnection problem in which multiple remote covariates $Z(r, t)$ impact a local spatio-temporal response $Y(s, t)$. The problem is further complicated as oftentimes local covariates $X(s, t)$ also impact the response.

Climate scientists often study teleconnections individually and without statistical tools that explicitly account for spatial dependence or local covariates. Although teleconnection studies often work with standardized anomaly data—data that have been normalized at each spatial location to remove the long-term mean and standard deviation—this transformation does not account for the short-term impact of local covariates. Many teleconnection studies also do not account for temporal dependence as they consider teleconnections on time scales that exceed the range of temporal autocorrelation. Researchers often use empirical orthogonal functions (EOF) (von Storch and Zwiers, 1999, chapter 13) with pointwise correlation maps and standard linear regressions, or

canonical correlation analysis (CCA) (von Storch and Zwiers, 1999, chapter 14) to characterize teleconnections. EOF is the term climate scientists use to refer to principal component analysis, and CCA is an analogous method to EOF introduced in Hotelling (1936) that relies on the singular value decomposition of the cross-covariance matrix $Cov(X, Y)$ of multivariate variables X and Y . Mantua et al. (1997) characterize the PDO using EOFs of Pacific Ocean sea surface temperatures to define a univariate PDO index time series (the score of the first principal component) that measures how strongly sea surface temperatures resemble historical conditions associated with PDO impacts. Pointwise correlations between the PDO index and local response variables, like precipitation at arbitrary United States locations, help quantify the PDO's impact. Ashok et al. (2007) use similar techniques to characterize a teleconnection distinct from ENSO, but still involving Pacific Ocean sea surface temperatures along the equator. Mo (2003) applies an ensemble version of CCA to use Pacific Ocean sea surface temperatures to predict precipitation across the United States. None of these models, however, explicitly account for spatial dependence or local covariates.

The teleconnection problem remains largely unaddressed in spatial statistics. Choi et al. (2015) propose an approach similar to CCA, in which the authors study teleconnections through cross-covariance matrices smoothed by spatial basis functions. This method does not include local covariates or specify a process model for teleconnection effects, and it is fit by minimizing the Frobenius norm between the empirical cross-covariance matrix and its smoothed estimate. Standard hierarchical spatial models, by comparison, often specify process models and are estimated using more robust Bayesian methods, but critically are not designed for teleconnection problems. Standard hierarchical spatial models (cf. Banerjee, Carlin and Gelfand, 2004, chapters 5-7, 10) assume data are observed on the same spatial domain, or—in spatial misalignment problems—on similar spatial domains. Since teleconnection literature leads us to anticipate that variability in some spatial datasets is partly caused by teleconnection effects, it is important to develop models that account for these physical phenomena.

We propose to address the teleconnection problem by introducing a geostatistical model that incorporates information from both local and remote covariates. We develop this model in the more general context of a spatial regression problem involving spatially disjoint covariates (Section 2), then apply it to a teleconnection case study (Section 3). We conclude with a brief discussion of the model and its possible extensions (Section 4), as well as directions for future work and application

(Section 5).

2. A geostatistical model for spatially disjoint covariates applied to teleconnections.

2.1. *Model formulation.* We extend typical geostatistical settings in which a local response variable $Y(\mathbf{s}, t) \in \mathbb{R}$ and covariate vector $\mathbf{x}(\mathbf{s}, t) \in \mathbb{R}^p$ are observed at locations $\mathbf{s} \in \mathcal{D}_Y \subseteq \mathbb{R}^2$ and timepoints $t \in \mathcal{T} = \{t_1, \dots, t_{n_t}\}$ to include remote covariates $z(\mathbf{r}, t) \in \mathbb{R}$ that are observed at spatially disjoint locations $\mathbf{r} \in \mathcal{D}_Z \subseteq \mathbb{R}^2$ s.t. $\mathcal{D}_Y \cap \mathcal{D}_Z = \emptyset$ and used in the spatial regression model

$$(1) \quad Y(\mathbf{s}, t) = \mathbf{x}^T(\mathbf{s}, t)\boldsymbol{\beta} + w(\mathbf{s}, t) + \varepsilon(\mathbf{s}, t) + \int_{\mathcal{D}_Z} \alpha(\mathbf{s}, \mathbf{r})z(\mathbf{r}, t)d\mathbf{r}$$

where regression coefficients $\boldsymbol{\beta} \in \mathbb{R}^p$, spatially correlated noise $w(\mathbf{s}, t)$, and independent noise $\varepsilon(\mathbf{s}, t)$ are standard components for spatial regression models. The remote covariate coefficients $\{\alpha(\mathbf{s}, \mathbf{r}) : \mathbf{s} \in \mathcal{D}_Y, \mathbf{r} \in \mathcal{D}_Z\}$ distinguish model (1) from existing geostatistical models (cf. [Banerjee, Carlin and Gelfand, 2004](#), chapters 5-7, 10) and provide a simple geostatistical framework for modeling teleconnections. These coefficients vary spatially and use the remote covariates defined on the disjoint spatial domain \mathcal{D}_Z to provide local adjustment to the mean. This provides a geostatistical approach to modeling teleconnections by augmenting a spatial regression model to incorporate information from spatially remote regions.

Geostatistical modeling conventions use mean zero Gaussian processes to specify the randomness of the spatially correlated components $w(\mathbf{s}, t)$ and $\alpha(\mathbf{s}, \mathbf{r})$, and an independent process to specify the noise $\varepsilon(\mathbf{s}, t)$ —the *nugget*. We complete the Gaussian process specifications by defining the covariance functions for the spatially correlated components. Let C_w and C_α respectively be the covariance functions for $w(\mathbf{s}, t) + \varepsilon(\mathbf{s}, t)$ and $\alpha(\mathbf{s}, \mathbf{r})$ and define them to be

$$(2) \quad C_w \{(\mathbf{s}, t), (\mathbf{s}', t')\} = (\kappa_s(\mathbf{s}, \mathbf{s}'; \boldsymbol{\theta}_w) + \sigma_\varepsilon^2 \delta_{\mathbf{s}, \mathbf{s}'}) \delta_{t, t'}$$

$$(3) \quad C_\alpha \{(\mathbf{s}, \mathbf{r}), (\mathbf{s}', \mathbf{r}')\} = (\kappa_s(\mathbf{s}, \mathbf{s}'; \boldsymbol{\theta}_w) + \sigma_\varepsilon^2 \delta_{\mathbf{s}, \mathbf{s}'}) \kappa_r(\mathbf{r}, \mathbf{r}'; \boldsymbol{\theta}_\alpha)$$

In these definitions, κ represents the Matérn covariance function, δ represents the Kronecker delta function, and the parameter vectors $\boldsymbol{\theta}_w = (\sigma_w^2, \rho_w, \nu_w)^T$ and $\boldsymbol{\theta}_\alpha = (\sigma_\alpha^2, \rho_\alpha, \nu_\alpha)^T$ respectively describe the variance, range, and smoothness of the Matérn covariances. Additionally, σ_ε^2 represents the variance of the nugget process which we specify to be a collection of independent and identically distributed mean zero Gaussian random variables; i.e., we let $\varepsilon(\mathbf{s}, t) \stackrel{iid}{\sim} \mathcal{N}(0, \sigma_\varepsilon^2)$.

The definitions for the covariances C_w and C_α can be generalized. The underlying covariance functions κ_w and κ_α do not need to be Matérn—any valid covariance function is acceptable. The definitions for C_w and C_α also induce a separable covariance structure for the remote coefficients, which could be relaxed to model additional spatio-temporal variation of the remote coefficient process $\alpha(\mathbf{s}, \mathbf{r})$.

2.2. Reduced rank approximation. Remote covariates $z(\mathbf{r}, t)$ in teleconnection applications will often be data that measure varied ocean properties at high spatial resolutions, like sea surface temperature or sea level pressure. This raises concerns for estimating model (1) as these covariates will vary smoothly and be highly collinear over \mathcal{D}_Z . Physically, the remote coefficients should also vary smoothly. We use predictive processes to mitigate multicollinearity in the remote covariates, marking a different motivation for predictive processes as [Banerjee et al. \(2008\)](#) originally introduce predictive processes to fit geostatistical models to large spatial datasets.

If the remote coefficient field $\alpha(\mathbf{s}, \cdot)$ varies smoothly at each local location $\mathbf{s} \in \mathcal{D}_Y$, then the remote coefficient $\alpha(\mathbf{s}, \mathbf{r})$ for remote location $\mathbf{r} \in \mathcal{D}_Z$ can be well represented by a weighted average of the field's value at knot locations $\mathbf{r}_1^*, \dots, \mathbf{r}_k^* \in \mathcal{D}_Z$. This lets us make the simplifying assumption that for some weight function $h(\mathbf{r}, \mathbf{r}')$ and vector of weights $\mathbf{h}^*(\mathbf{r}) = [h(\mathbf{r}, \mathbf{r}_j^*)]_{j=1}^k \in \mathbb{R}^k$ we can write

$$(4) \quad \alpha(\mathbf{s}, \mathbf{r}) = \sum_{j=1}^k h(\mathbf{r}, \mathbf{r}_j^*) \alpha(\mathbf{s}, \mathbf{r}_j^*) = \mathbf{h}^*(\mathbf{r})^T \boldsymbol{\alpha}^*(\mathbf{s})$$

in which $\boldsymbol{\alpha}^*(\mathbf{s}) = [\alpha(\mathbf{s}, \mathbf{r}_j^*)]_{j=1}^k \in \mathbb{R}^k$. The predictive process approach uses kriging to motivate a choice for the weight vector $\mathbf{h}^*(\mathbf{r})$ which will induce an associated weight function h . The Gaussian process assumption made in Section 2.1 about the remote coefficient field implies that $\alpha(\mathbf{s}, \mathbf{r})$ and $\boldsymbol{\alpha}^*(\mathbf{s})$ are jointly normally distributed, yielding the conditional expectation for $\alpha(\mathbf{s}, \mathbf{r})$

$$(5) \quad E[\alpha(\mathbf{s}, \mathbf{r}) | \boldsymbol{\alpha}^*(\mathbf{s})] = \mathbf{c}^*(\mathbf{r})^T R^{*-1} \boldsymbol{\alpha}^*(\mathbf{s})$$

in which $\mathbf{c}^*(\mathbf{r}) = [C_\alpha\{(\mathbf{s}, \mathbf{r}), (\mathbf{s}, \mathbf{r}_j^*)\}]_{j=1}^k \in \mathbb{R}^k$ and $R^* = [C_\alpha\{(\mathbf{s}, \mathbf{r}_i^*), (\mathbf{s}, \mathbf{r}_j^*)\}]_{i,j=1}^k \in \mathbb{R}^{k \times k}$. The choice of notation for the vector $\mathbf{c}^*(\mathbf{r})$ and matrix R^* highlights the consequence that defining C_α with stationary covariance functions means $\mathbf{c}^*(\mathbf{r})$ and R^* do not depend on \mathbf{s} , despite the term appearing in their definitions.

The predictive process approach uses the conditional expectation (5) to motivate defining the weight vector $\mathbf{h}^*(\mathbf{r}) = \mathbf{c}^*(\mathbf{r})^T R^{*-1}$ in the approximation (4). Banerjee et al. (2008) show that these types of approximations are optimal reduced rank projections that can capture key spatial structures in data. Additionally, we find this approach has a natural interpretation when model (1) is applied to finite samples.

With n_r remote locations $r_1, \dots, r_{n_r} \in \mathcal{D}_Z$ the integral in (1) simplifies to a finite sum that the reduced rank approximation lets us manipulate:

$$\begin{aligned} \sum_{i=1}^{n_r} \alpha(\mathbf{s}, \mathbf{r}_i) z(\mathbf{r}_i, t) &= \sum_{i=1}^{n_r} \left(\sum_{j=1}^k h(\mathbf{r}_i, \mathbf{r}_j^*) \alpha(\mathbf{s}, \mathbf{r}_j^*) \right) z(\mathbf{r}_i, t) \\ &= \sum_{j=1}^k \alpha(\mathbf{s}, \mathbf{r}_j^*) \left(\sum_{i=1}^{n_r} h(\mathbf{r}_i, \mathbf{r}_j^*) z(\mathbf{r}_i, t) \right) \\ &= \sum_{j=1}^k \alpha(\mathbf{s}, \mathbf{r}_j^*) z^*(\mathbf{r}_j^*, t) \end{aligned}$$

where $z^*(\mathbf{r}_j^*, t) = \sum_{i=1}^{n_r} h(\mathbf{r}_i, \mathbf{r}_j^*) z(\mathbf{r}_i, t)$. This brief manipulation demonstrates how using the predictive process approach to address multicollinearity in the remote covariates is analogous to replacing the n_r remote covariates $z(\cdot, t)$ at each timepoint with k weighted-average indices $z^*(\cdot^*, t)$ that reduce the dimension of the remote covariate field by summarizing it with k zonal averages. As the weights are based on standard covariance functions, these indices will be localized in the sense that the index value $z^*(\mathbf{r}_j^*, t)$ will be most influenced by $z(\mathbf{r}, t)$ for nearby \mathbf{r} .

2.3. Model likelihood. The data likelihood is jointly normal for finite samples with n_s locations, n_r remote locations, and n_t timepoints. Let the vectors $\mathbf{Y}_t = [Y(\mathbf{s}_i, t)]_{i=1}^{n_s} \in \mathbb{R}^{n_s}$ and $\mathbf{z}_t = [z(\mathbf{r}_j, t)]_{j=1}^{n_r} \in \mathbb{R}^{n_r}$, and the matrix $X_t = [\mathbf{x}(\mathbf{s}_i, t)^T]_{i=1}^{n_s} \in \mathbb{R}^{n_s \times p}$ represent the observed response variables and covariates at time t , and let the vector $\boldsymbol{\alpha}(\mathbf{s}) = [\alpha(\mathbf{s}, \mathbf{r}_j)]_{j=1}^{n_r} \in \mathbb{R}^{n_r}$ represent the teleconnection coefficients for location \mathbf{s} . Each timepoint t has the data likelihood

$$(6) \quad \mathbf{Y}_t | \boldsymbol{\beta}, \tilde{\boldsymbol{\alpha}}, \Sigma \sim \mathcal{N}\left(X_t \boldsymbol{\beta} + \tilde{Z}_t \tilde{\boldsymbol{\alpha}}, \Sigma\right)$$

where $\tilde{Z}_t = I_{n_s} \otimes \mathbf{z}_t^T$, $\tilde{\boldsymbol{\alpha}} = [\boldsymbol{\alpha}(\mathbf{s}_i)]_{i=1}^{n_s} \in \mathbb{R}^{n_s n_r}$, $\Sigma = [C_w\{(\mathbf{s}_i, t), (\mathbf{s}_j, t)\}]_{i,j=1}^{n_s} \in \mathbb{R}^{n_s \times n_s}$, and \otimes denotes the Kronecker product. The remote effects term $\tilde{Z}_t \tilde{\boldsymbol{\alpha}} = [\mathbf{z}_t^T \boldsymbol{\alpha}(\mathbf{s}_i)]_{i=1}^{n_s} \in \mathbb{R}^{n_s}$ shows that $Y(\mathbf{s}_1, t), \dots, Y(\mathbf{s}_{n_s}, t)$ share the same covariates \mathbf{z}_t and more clearly illustrates how the disjoint covariates model (1) differs from existing spatial models—especially those that include spatially

varying effects (cf. [Banerjee, Carlin and Gelfand, 2004](#), section 10.2). Although the remote coefficients in model (1) vary spatially across \mathcal{D}_Y , the covariates with which they are paired do not.

The entire dataset of n_t timepoints has the data likelihood

$$(7) \quad \mathbf{Y} = \left(\mathbf{Y}_{t_1}^T \dots \mathbf{Y}_{t_{n_t}}^T \right)^T \Big| \boldsymbol{\beta}, \tilde{\boldsymbol{\alpha}}, \Sigma \sim \mathcal{N} \left(\tilde{\mathbf{X}} (\mathbf{1}_{n_t} \otimes \boldsymbol{\beta}) + \tilde{\mathbf{Z}} (\mathbf{1}_{n_t} \otimes \tilde{\boldsymbol{\alpha}}), I_{n_t} \otimes \Sigma \right)$$

where $\tilde{\mathbf{X}} = \text{diag} \{ X_{t_1}, \dots, X_{t_{n_t}} \}$ and $\tilde{\mathbf{Z}} = \text{diag} \{ \tilde{Z}_{t_1}, \dots, \tilde{Z}_{t_{n_t}} \}$ are block diagonal matrices of the observed covariates. While this notation is convenient for writing likelihoods for model (1), it is not convenient for numerically evaluating these likelihoods. Section 2.4 introduces more convenient notation when describing a Gibbs sampler that estimates model parameters.

Adopting the reduced rank assumption lets us use notation from Section 2.2 to rewrite $\boldsymbol{\alpha}(\mathbf{s}) = \mathbf{c}^* R^{*-1} \boldsymbol{\alpha}^*(\mathbf{s})$ by defining the matrix $\mathbf{c}^* = \left[\mathbf{c}^* (r_j)^T \right]_{j=1}^{n_r} \in \mathbb{R}^{n_r \times k}$. This implies $\tilde{\boldsymbol{\alpha}} = (I_{n_s} \otimes \mathbf{c}^* R^{*-1}) \tilde{\boldsymbol{\alpha}}^*$, which yields modified versions of likelihoods (6) and (7):

$$(8) \quad \mathbf{Y}_t | \boldsymbol{\beta}, \tilde{\boldsymbol{\alpha}}^*, R^*, \mathbf{c}^*, \Sigma \sim \mathcal{N} \left(X_t \boldsymbol{\beta} + \tilde{Z}_t^* \tilde{\boldsymbol{\alpha}}^*, \Sigma \right)$$

$$(9) \quad \mathbf{Y} = \left(\mathbf{Y}_{t_1}^T \dots \mathbf{Y}_{t_{n_t}}^T \right)^T \Big| \boldsymbol{\beta}, \tilde{\boldsymbol{\alpha}}^*, R^*, \mathbf{c}^*, \Sigma \sim \mathcal{N} \left(\tilde{\mathbf{X}} (\mathbf{1}_{n_t} \otimes \boldsymbol{\beta}) + \tilde{\mathbf{Z}}^* (\mathbf{1}_{n_t} \otimes \tilde{\boldsymbol{\alpha}}^*), I_{n_t} \otimes \Sigma \right)$$

in which $\tilde{\boldsymbol{\alpha}}^* = [\boldsymbol{\alpha}^*(\mathbf{s}_i)]_{i=1}^{n_s} \in \mathbb{R}^{n_s k}$, $\tilde{Z}_t^* = I_{n_s} \otimes \mathbf{z}_t^{*T}$, and $\tilde{\mathbf{Z}}^* = \text{diag} \{ \tilde{Z}_{t_1}^*, \dots, \tilde{Z}_{t_{n_t}}^* \}$ where $\mathbf{z}_t^{*T} = \mathbf{z}_t^T \mathbf{c}^* R^{*-1}$. The model is completely specified for a Bayesian analysis by defining prior distributions for model parameters.

2.4. Bayesian implementation. We adopt a hierarchical Bayesian framework to estimate parameters and make predictions for model (9). We use conjugate prior distributions where possible, setting $\boldsymbol{\beta} \sim \mathcal{N}(\mathbf{0}, \boldsymbol{\Lambda})$ for some fixed prior covariance matrix $\boldsymbol{\Lambda}$, and $\sigma_w^2 \sim IG(a_{\sigma_w^2}, b_{\sigma_w^2})$. We use standard choices for weakly informative priors for remaining parameters: $\sigma_{\alpha}^2 \sim IG(a_{\sigma_{\alpha}^2}, b_{\sigma_{\alpha}^2})$, $\sigma_{\varepsilon}^2 \sim IG(a_{\sigma_{\varepsilon}^2}, b_{\sigma_{\varepsilon}^2})$, $\rho_w \sim U(a_{\rho_w}, b_{\rho_w})$, and $\rho_{\alpha} \sim U(a_{\rho_{\alpha}}, b_{\rho_{\alpha}})$ ([Banerjee et al., 2008](#)). As spatial smoothness parameters are difficult to estimate in standard applications, we estimate ν_w and ν_{α} from sample variograms and treat these parameters as fixed during model fitting. The Gaussian process assumption for $\alpha(\cdot, \cdot)$ implies the remote coefficients have prior distribution

$$(10) \quad \tilde{\boldsymbol{\alpha}}^* | \Sigma, R^* \sim \mathcal{N}(\mathbf{0}, \Sigma \otimes R^*)$$

The Kronecker form for the remote coefficient covariance matrix follows from defining C_{α} as a separable covariance function, implying the model's teleconnection coefficients are spatially correlated over the remote region \mathcal{D}_Z and that these fields vary smoothly between nearby locations in \mathcal{D}_Y .

Bayesian estimation is often more stable after integrating out latent fields (Banerjee, Carlin and Gelfand, 2004, pg. 127). The marginalized likelihood for the entire dataset of n_t timepoints after integrating out $\tilde{\boldsymbol{\alpha}}^*$ is

$$(11) \quad \mathbf{Y} | \boldsymbol{\beta}, R^*, \mathbf{c}^*, \Sigma \sim \mathcal{N} \left(\tilde{\mathbf{X}} (\mathbf{1}_{n_t} \otimes \boldsymbol{\beta}), C^{-1} \otimes \Sigma \right)$$

where $C^{-1} = I_{n_t} + \mathbf{Z}^{*T} R^* \mathbf{Z}^*$ and $\mathbf{Z}^* = [\mathbf{z}_{t_1}^* \dots \mathbf{z}_{t_{n_t}}^*] \in \mathbb{R}^{k \times n_t}$ is a dense matrix that contains the remote covariates. Since the Kronecker product is a bilinear operator, the marginalized variance $C^{-1} \otimes \Sigma$ decomposes into the sum $(I_{n_t} \otimes \Sigma) + (\mathbf{Z}^{*T} R^* \mathbf{Z}^* \otimes \Sigma)$ which more clearly highlights how the remote covariates account for some of the spatial variability around the fixed mean $\tilde{\mathbf{X}} (\mathbf{1}_{n_t} \otimes \boldsymbol{\beta})$.

Further studying the marginalized likelihood (11) reveals that the model parameters are identifiable with the exception that σ_ε^2 is only identifiable up to its product with σ_w^2 . We use parameter expansion to fit this model by reparameterizing the nugget variance as $\sigma_\varepsilon^2 = \sigma_w^2 \tilde{\sigma}_\varepsilon^2$ and estimating $\tilde{\sigma}_\varepsilon^2$ instead of estimating σ_ε^2 directly.

Model fitting employs a hybrid Gibbs sampler with adaptive random walk Metropolis steps to estimate parameters for the marginalized likelihood (11). Sampling proceeds by updating the regression coefficient and spatial variance parameters $\boldsymbol{\beta}$ and σ_w^2 by drawing from their conjugate posterior distributions

$$(12) \quad \boldsymbol{\beta} | \cdot \sim \mathcal{N} (\Sigma_{\boldsymbol{\beta} | \cdot} \mathbf{X}^T (C \otimes \Sigma^{-1}) \mathbf{Y}, \Sigma_{\boldsymbol{\beta} | \cdot})$$

$$(13) \quad \sigma_w^2 | \cdot \sim IG \left(a_{\sigma_w^2} + n_s n_t / 2, b_{\sigma_w^2} + e^T [C \otimes (\Sigma / \sigma_w^2)^{-1}] e / 2 \right)$$

where $\mathbf{X} = [X_{t_1}^T \dots X_{t_{n_t}}^T]^T \in \mathbb{R}^{n_s n_t \times p}$ is a dense matrix that contains the covariates measured across \mathcal{D}_Y , $e = (\mathbf{Y} - \tilde{\mathbf{X}} (\mathbf{1}_{n_t} \otimes \boldsymbol{\beta}))$ are the model residuals, and

$$(14) \quad \Sigma_{\boldsymbol{\beta} | \cdot} = \{\boldsymbol{\Lambda}^{-1} + \mathbf{X}^T (C \otimes \Sigma^{-1}) \mathbf{X}\}^{-1}$$

is the posterior covariance matrix for $\boldsymbol{\beta}$. The remaining parameters ρ_w , ρ_α , σ_α^2 , and $\tilde{\sigma}_\varepsilon^2$ are transformed to unconstrained supports and updated using adaptive random walk Metropolis steps with normal proposals. Log transformations are used for the positive parameters σ_α^2 and $\tilde{\sigma}_\varepsilon^2$, and logit transformations are used for the bounded parameters ρ_w and ρ_α . The adaptive proposal variance $\lambda(\cdot)$ differs for each parameter and is tuned at each iteration following a basic version of algorithm 4 from Andrieu and Thoms (2008). This algorithm specifies the adaptation formula

$$\log \lambda(\cdot) = \log \lambda(\cdot) + \gamma(\alpha(\cdot) - \alpha^*(\cdot))$$

for some fixed adaptation step size γ . The adaptation formula implements a Robbins-Monro algorithm that tunes the proposal variance $\lambda(\cdot)$ so that the MCMC acceptance rate for each parameter $\alpha(\cdot)$ converges to a desired acceptance rate $\alpha^*(\cdot)$ while ensuring that the MCMC chain still converges to the sampled parameters' posterior distribution. Additional computations, however, are required to estimate the remote coefficients and make predictions.

Composition sampling (Banerjee, Carlin and Gelfand, 2004, p. 132) provides a means to sample from the posterior distribution of the remote coefficients $\tilde{\alpha}^*$ as well as from the posterior predictive distribution of the response variables \mathbf{Y}_{t_0} at a new timepoint t_0 . This allows inference and prediction of these processes, which the Gibbs sampler does not directly study. Composition sampling approximates the posterior distribution of $\tilde{\alpha}^*$ by averaging the conditional posterior distribution for $\tilde{\alpha}^*$ over posterior samples obtained by Gibbs sampling. The approximation relies on Monte Carlo integration ideas, so the marginal posterior distribution of $\tilde{\alpha}^*$ is written as

$$\begin{aligned} p(\tilde{\alpha}^* | \mathbf{Y}) &= \int p(\tilde{\alpha}^* | \mathbf{Y}, \boldsymbol{\beta}, \boldsymbol{\theta}_w, \boldsymbol{\theta}_\alpha, \sigma_\varepsilon^2) p(\boldsymbol{\beta}, \boldsymbol{\theta}_w, \boldsymbol{\theta}_\alpha, \sigma_\varepsilon^2 | \mathbf{Y}) d(\boldsymbol{\beta}, \boldsymbol{\theta}_w, \boldsymbol{\theta}_\alpha, \sigma_\varepsilon^2) \\ &\approx \frac{1}{G} \sum_{g=1}^G p(\tilde{\alpha}^* | \mathbf{Y}, \boldsymbol{\beta}^{(g)}, \boldsymbol{\theta}_w^{(g)}, \boldsymbol{\theta}_\alpha^{(g)}, \sigma_\varepsilon^{2(g)}) \end{aligned}$$

where—for example— $\boldsymbol{\beta}^{(g)}$ represents the g -th posterior sample of $\boldsymbol{\beta}$ drawn from the Gibbs sampler. In practice, $p(\tilde{\alpha}^* | \mathbf{Y})$ is approximated by sampling $\{\tilde{\alpha}^{*(1)}, \dots, \tilde{\alpha}^{*(G)}\}$ in which each composition sample $\tilde{\alpha}^{*(g)}$ is drawn from the conditional posterior distribution for $\tilde{\alpha}^{*(g)}$:

$$(15) \quad \tilde{\alpha}^{*(g)} | \cdot \sim \mathcal{N}(\boldsymbol{\mu}_{\tilde{\alpha}^{*(g)}} | \cdot, \Sigma_{\tilde{\alpha}^{*(g)}} | \cdot)$$

in which

$$\begin{aligned} \boldsymbol{\mu}_{\tilde{\alpha}^{*(g)}} | \cdot &= \sum_{t \in \mathcal{T}} \left\{ \left(\mathbf{Y}_t - \mathbf{X}_t \boldsymbol{\beta}^{(g)} \right) \otimes \left(R^{*-1(g)} + \mathbf{Z}^{*(g)} \mathbf{Z}^{*(g)T} \right)^{-1} \mathbf{z}_t^{*(g)} \right\} \\ \Sigma_{\tilde{\alpha}^{*(g)}} | \cdot &= \Sigma^{(g)} \otimes \left(R^{*-1(g)} + \mathbf{Z}^{*(g)} \mathbf{Z}^{*(g)T} \right)^{-1} \end{aligned}$$

The Kronecker structure of $\boldsymbol{\mu}_{\tilde{\alpha}^{*(g)}} | \cdot$ and $\Sigma_{\tilde{\alpha}^{*(g)}} | \cdot$ allows the posterior distribution of the remote coefficients to be studied more closely. Recalling that $\tilde{\alpha}^* = [\alpha^*(\mathbf{s}_i)]_{i=1}^{n_s} \in \mathbb{R}^{n_s k}$ and exploiting the multivariate normal distribution's marginal distribution properties implies

$$(16) \quad \alpha^*(\mathbf{s})^{(g)} | \cdot \sim \mathcal{N}(\boldsymbol{\mu}_{\alpha^*(\mathbf{s})^{(g)}} | \cdot, \Sigma_{\alpha^*(\mathbf{s})^{(g)}} | \cdot)$$

in which $\Sigma_{\mathbf{s}, \mathbf{s}}^{(g)}$ is the s^{th} diagonal entry in $\Sigma^{(g)}$ and

$$(17) \quad \boldsymbol{\mu}_{\boldsymbol{\alpha}^*(\mathbf{s})^{(g)}}|_{\cdot} = \left(R^{*-1(g)} + \mathbf{Z}^{*(g)} \mathbf{Z}^{*(g)T} \right)^{-1} \sum_{t \in \mathcal{T}} \left(Y(\mathbf{s}, t) - \mathbf{x}(\mathbf{s}, t)^T \boldsymbol{\beta}^{(g)} \right) \mathbf{z}_t^{*(g)}$$

$$(18) \quad \Sigma_{\boldsymbol{\alpha}^*(\mathbf{s})^{(g)}}|_{\cdot} = \Sigma_{\mathbf{s}, \mathbf{s}}^{(g)} \left(R^{*-1(g)} + \mathbf{Z}^{*(g)} \mathbf{Z}^{*(g)T} \right)^{-1}$$

With manipulations detailed in Appendix A, this distributional form is equivalent to the posterior distribution of a Bayesian linear regression of the local residuals over time $\left[Y(\mathbf{s}, t) - \mathbf{x}(\mathbf{s}, t)^T \boldsymbol{\beta}^{(g)} \right]_{t=1}^{n_t} \in \mathbb{R}^{n_t}$ onto the remote covariates $\mathbf{Z}^{*(g)T}$ when using a prior mean of $\mathbf{0}$ and prior covariance matrix $\Sigma_{\mathbf{s}, \mathbf{s}}^{(g)} R^{*(g)}$. This suggests that patterns in maps of posterior means of $\tilde{\boldsymbol{\alpha}}^*$ can resemble patterns in maps that show pointwise correlations between $z^*(\mathbf{r}^*, \cdot)$ and $Y(\mathbf{s}, \cdot)$.

2.5. Variance inflation factors. The posterior covariance matrix (14) for the regression coefficient vector $\boldsymbol{\beta}$ allows us to follow [Reich, Hodges and Zadnik \(2006\)](#) and define conditional variance inflation factors (VIFs) that can help diagnose multicollinearity issues between the local and remote covariate matrices \mathbf{X} and \mathbf{Z} :

$$(19) \quad VIF(\beta_i) = \frac{\left(\{\boldsymbol{\Lambda}^{-1} + \mathbf{X}^T (C \otimes \Sigma^{-1}) \mathbf{X}\}^{-1} \right)_{ii}}{\left(\{\boldsymbol{\Lambda}^{-1} + \mathbf{X}^T (I_{n_t} \otimes \Sigma^{-1}) \mathbf{X}\}^{-1} \right)_{ii}}$$

The VIF measures the proportional increase in the i^{th} local coefficient's posterior variance caused by adding remote covariates to the model, conditional on the model's covariance parameters. This interpretation follows since the denominator represents the i^{th} local coefficient's posterior covariance in a standard spatial regression model that observes the local covariate and response fields at multiple, independent timepoints. Larger VIF values indicate greater multicollinearity issues, while the smallest possible VIF value of 1 indicates no multicollinearity. The derivation of the lower bound of (19) is included in Appendix B.

2.6. Computational approach for conducting inference on remote coefficients. The composition samples $\{\tilde{\boldsymbol{\alpha}}^{*(1)}, \dots, \tilde{\boldsymbol{\alpha}}^{*(G)}\}$ in (15) are independent given the posterior parameter samples. This allows these samples to be drawn in parallel, thereby reducing the amount of real time needed to conduct inference on $\tilde{\boldsymbol{\alpha}}^*$. However, memory constraints make conducting inference on $\tilde{\boldsymbol{\alpha}}^*$ difficult.

The composition sampling scheme described in Section 2.4 that estimates the remote coefficients' posterior distribution $p(\tilde{\boldsymbol{\alpha}}^* | \mathbf{Y})$ requires storing $n_s \times k \times G$ floating point numbers. Even for moderately sized studies with $n_s = 200$, $k = 30$, and $G = 20,000$, composition sampling requires 915MB

of memory. Although this demand increases linearly in k and n_s , or as one attempts to use the deterministic relationship between $\tilde{\alpha}^*$ and $\tilde{\alpha}$ to conduct inference on $\tilde{\alpha}$ (which requires storing $n_s \times n_r \times G$ floating point numbers), this demand quickly becomes burdensome for typical personal computers. We therefore conduct inference on $\tilde{\alpha}^*$ using the normal approximation to the posterior. The normal approximation only requires the composition sample's mean $\hat{\mu}_{\tilde{\alpha}|\mathbf{Y}} = \frac{1}{G} \sum_{g=1}^G \tilde{\alpha}^{*(g)}$ and covariance matrix $\hat{\Sigma}_{\tilde{\alpha}|\mathbf{Y}} = \frac{1}{G-1} \sum_{g=1}^G \left(\tilde{\alpha}^{*(g)} - \hat{\mu}_{\tilde{\alpha}|\mathbf{Y}} \right) \left(\tilde{\alpha}^{*(g)} - \hat{\mu}_{\tilde{\alpha}|\mathbf{Y}} \right)^T$. These objects require storing $(n_s \times k)(n_s \times k + 1)$ floating point numbers, which can dramatically reduce memory requirements when $G > n_s \times k + 1$.

[Pébay \(2008, eqs. 1.3 & 3.11\)](#) presents formulas that can use partitions of the composition samples to compute $\hat{\mu}_{\tilde{\alpha}|\mathbf{Y}}$ and $\hat{\Sigma}_{\tilde{\alpha}|\mathbf{Y}}$, which facilitates estimating $p(\tilde{\alpha}^*|\mathbf{Y})$ in parallel and with minimal memory requirements. [Pébay \(2008, eqs. 1.1 & 3.12\)](#) additionally presents formulas that can also compute $\hat{\mu}_{\tilde{\alpha}|\mathbf{Y}}$ and $\hat{\Sigma}_{\tilde{\alpha}|\mathbf{Y}}$ in a streaming context, which further reduces memory requirements. These benefits are achieved by recognizing, for example, that a running estimate of $\hat{\mu}_{\tilde{\alpha}|\mathbf{Y}}$ based on $\{\tilde{\alpha}^{*(1)}, \dots, \tilde{\alpha}^{*(g)}\}$ is easy to update when the next composition sample $\tilde{\alpha}^{*(g+1)}$ is drawn and that the updating equations yield $\hat{\mu}_{\tilde{\alpha}|\mathbf{Y}}$ once all G composition samples are processed.

3. Case study. Pacific Ocean sea surface temperatures influence seasonal precipitation in Florida through several teleconnections ([Douglas and Englehart, 1981](#); [Misra and DiNapoli, 2013](#); [Ashok et al., 2007](#); [Mantua et al., 1997](#)). However, local covariates are also critical for determining precipitation ([Daly et al., 2008](#)). Statistical models that account for local and remote covariates should yield better predictions than models that only consider local or remote covariates, but not both. We use the geostatistical model for spatially disjoint covariates described in Section 2 to use Pacific Ocean sea surface temperatures as remote covariates with additional local covariates to improve predictions of Winter precipitation in Florida. Simplifications of the disjoint covariate model (1) that only incorporate either local or remote covariates—but not both—serve as comparison models.

3.1. Data. This study uses the ERA-Interim reanalysis dataset to provide sea surface temperatures and local covariates ([Dee et al., 2011](#)). The response data, precipitation, comes from the PRISM dataset ([Daly et al., 2008](#)). Both datasets are reanalysis products, which are necessary because working directly with observations can be challenging since data may be from various

sources, and are often spatially sparse and temporally incomplete. As such, reanalysis products use statistical techniques and physical relationships to reproduce consistent datasets at regular, gridded locations with complete records.

This study analyzes data for winter months (December, January, February) from 1981 through 2013. Seasonal average monthly precipitation (P) in Florida, the response variable, is studied with respect to local covariates: seasonal average surface temperature (T), total column water vapor ($TCWV$), and geopotential height of the 700hPa pressure level (Z_{700}). Pacific Ocean sea surface temperatures (SST) between 120°E – 70°W and 20°S – 60°N are also included as remote covariates. The data are spatially aggregated so that 263 28km-resolution grid cells cover Florida and 350 345km-resolution grid cells cover the Pacific Ocean. The dataset is partitioned by year into training and test datasets. The model is fit using 25 years of data and its accuracy is assessed with the remaining 8 years of data. The assessment years are 1983–85, 1993, 2000, 2002, 2005, and 2007. These years were selected randomly, but so that the distribution of annual precipitation variability across Florida, $Var(P(\cdot, t))$, is similar between the training and test datasets.

All data are converted to standardized anomalies before analysis. The standardized anomaly for a variable X at a location s and time t represents the number of standard deviations $X(s, t)$ is above or below the average value of X at location s .

3.2. Model and prior specification. We use a simple, linear model to relate the local covariates (T , $TCWV$, Z_{700}) to the response, precipitation (P). Equation (20) presents the mean equation for the fixed effects of the local covariates:

$$(20) \quad E[P(s, t)] = \beta_0 + \beta_T T(s, t) + \beta_{TCWV} TCWV(s, t) + \beta_{Z_{700}} Z_{700}(s, t)$$

Remote coefficient knots are placed at 28 locations that are roughly evenly spaced across the Pacific Ocean and along coastal locations. Knot locations are plotted in [Figure 2](#). These locations are dense enough to capture sea surface temperature variability, but sparse enough to minimize potential multicollinearity issues. While knot selection can be problematic, [Banerjee et al. \(2008\)](#) find that reasonably dense, regularly spaced grids can yield good results.

We adopt a combination of weakly informative and uninformative prior distributions. The prior covariance matrix for the fixed effects β is diagonal and sets the prior variance for each β_i equal to $10 \times Var(X_i(\cdot, \cdot))$. We use $\sigma_w^2 \sim IG(2, 30)$, $\sigma_\alpha^2 \sim IG(2, 1)$, $\sigma_\varepsilon^2 \sim IG(2, 1)$, $\rho_w \sim U(1, 600)$, and

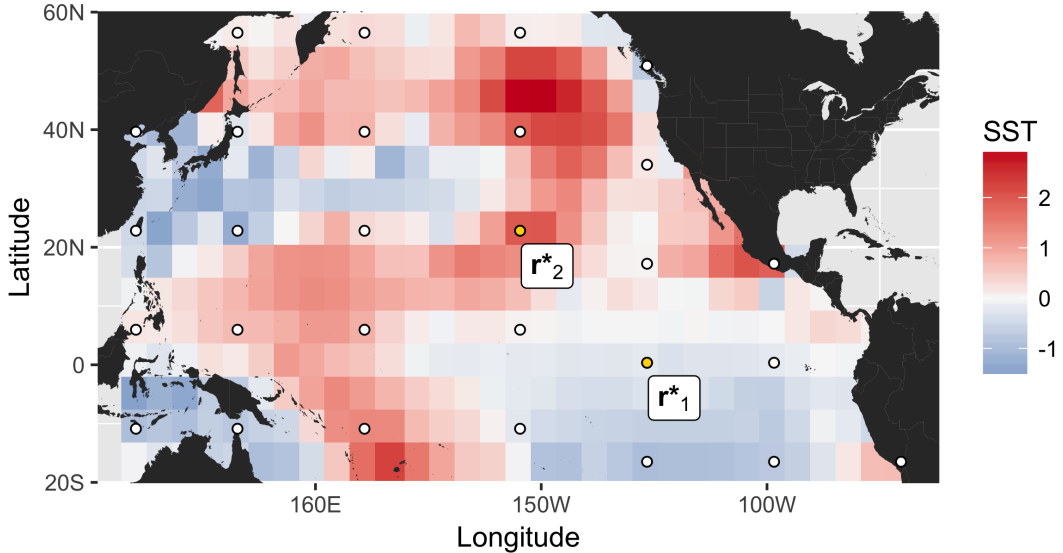


Fig 2: Average monthly sea surface temperature standardized anomalies from Winter, 2013. White dots with black outlines mark remote coefficient knot locations. Section 3.3.1 and Figure 3 discuss the two labeled, yellow-highlighted knot locations r_1^* and r_2^* .

$\rho_\alpha \sim U(1, 600)$. The covariance smoothness parameters are fixed at $\nu_w = 2$ and $\nu_\alpha = 1.76$, which were determined by inspecting variograms for the local and remote data.

3.3. Results. Model results are based on 19,000 samples from the posterior distribution after a burn in period of 1,000 samples. Convergence was assessed by examining traceplots, autocorrelation plots, and effective sample sizes in addition to comparing results from multiple runs with randomly initialized parameters. Model adequacy was assessed using residual and qq-normal plots. These diagnostics suggest that convergence and distributional assumptions hold.

3.3.1. Inference. Parameter estimates for the full disjoint covariate model (1), which uses both local covariates and Pacific Ocean sea surface temperatures, are reported in Table 1. The sign of the regression coefficients are consistent with physical processes that influence precipitation. Variance inflation factors for the regression coefficients, computed at the posterior mean for all parameters, suggest these data do not suffer from multicollinearity issues caused by the remote covariates. The local covariance range parameter ρ_w implies the dependence between locations $s \in \mathcal{D}_Y$ has an effective range between 230km and 250km. This range is suggestive of mesoscale processes, which

Table 1: Posterior mean estimates and 95% HPD intervals for model parameters. Variance inflation factors (VIF) computed at the posterior mean are also included for regression parameters. Significant regression parameters are highlighted in bold.

	Posterior mean	95% HPD	VIF
β_0	-0.019	(-0.068, 0.031)	1.1
β_{TCWV}	0.459	(0.387, 0.532)	1.4
β_T	0.042	(-0.037, 0.123)	1.4
$\beta_{Z_{700}}$	-0.703	(-0.779, -0.629)	1.6
σ_w^2	0.165	(0.155, 0.174)	
σ_α^2	0.01	(0.009, 0.011)	
$\tilde{\sigma}_\varepsilon^2$	0.066	(0.062, 0.071)	
ρ_w	27.929	(26.955, 28.902)	
ρ_α	24.046	(6.053, 39.859)	

include various phenomena that produce precipitation (Parker, 2015). The remote covariance range parameter ρ_α is less well estimated and implies the dependence between remote coefficients—for example, between $\alpha(\mathbf{s}, \mathbf{r}_i^*)$ and $\alpha(\mathbf{s}, \mathbf{r}_j^*)$ —have an effective range between 40km and 330km. This range is still suggestive of mesoscale processes, but is much less specific. There are concerns about convergence issues related to ρ_α and σ_α^2 . We are considering improvements to the model to address this.

The disjoint covariate model (1) can reproduce known teleconnection patterns and can also investigate the potential for new, currently unknown teleconnections. Florida’s precipitation is influenced by tropical sea surface temperatures (Douglas and Englehart, 1981), including the Niño 3.4 region (Trenberth, 1997). The plot on the left in Figure 3 shows the model reproduces this known teleconnection result, while the plot on the right shows a potentially influential pattern that is not associated with known teleconnections. Towler, PaiMazumder and Holland (2016) show that studying local precipitation can help identify previously unknown teleconnections.

3.3.2. Prediction. The disjoint covariate model’s fit is evaluated by its ability to predict Winter precipitation on the test dataset. In addition to evaluating predictions made with both the local and remote covariates, we use simplified versions of the the disjoint covariate model (1) to create

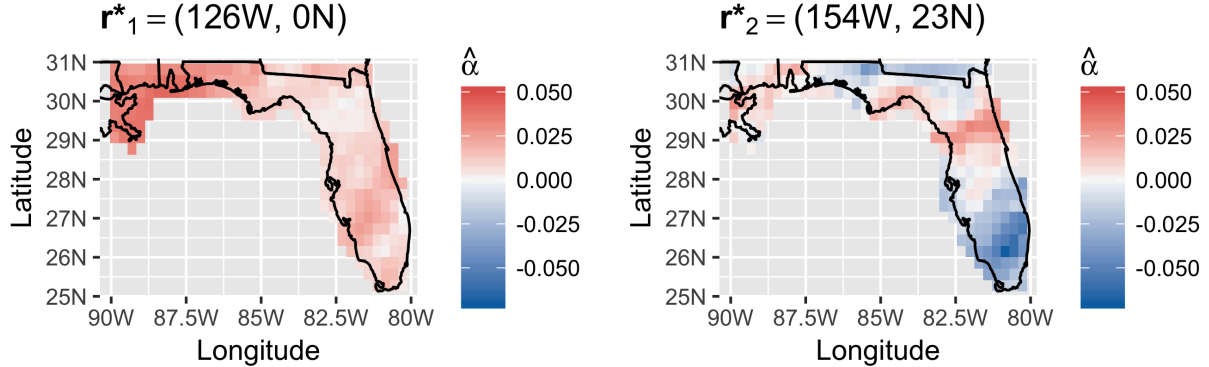


Fig 3: Estimated teleconnection effects for the knot locations r^* highlighted in [Figure 2](#). The plot on the left (r_1^*) shows teleconnection coefficients associated with an area in the Niño 3.4 region ([Trenberth, 1997](#)). This teleconnection pattern is consistent with the tendency for Florida precipitation to increase in El Niño events, during which Niño 3.4 sea surface temperatures increase. The plot on the right (r_2^*) shows teleconnection coefficients associated with an area near the Hawaiian islands. The pattern is not associated with known teleconnections.

two additional sets of predictions: one set of predictions that only use the local covariates, and another set that only use the remote covariates. These additional predictions let us compare the disjoint covariate model (1) with standard geostatistical modeling approaches that only use local covariates, and also with approaches in teleconnection studies that focus on remote covariates.

One common approach to evaluating precipitation predictions is to use categorical forecasts at each grid cell that predict the terciles “Above average”, “Near average”, or “Below average” standardized anomaly precipitation levels instead of mean quantities with confidence intervals. Prediction categories represent the posterior mode of the discretized posterior predictive distribution for each location and timepoint, although probabilistic forecasts could be used instead. Category cut points differ for each location and are set at each location’s precipitation terciles that are empirically determined from the training data.

The Heidke skill score (HS) measures categorical forecast accuracy and is commonly used in

climate sciences. [von Storch and Zwiers \(1999, section 18.1\)](#) review this measure's definition and some of its beneficial properties. The measure compares the probability that the full disjoint covariate model (1) makes a correct prediction p_F to the probability that a reference model makes a correct prediction p_E . We adopt a standard, naive reference model that assigns equal probability to precipitation categories, implying $p_E = 1/3$. We additionally manipulate the Heidke skill score formula ([von Storch and Zwiers, 1999, eq. 18.1](#)) so we may offer an intuitive interpretation for the score:

$$HS \triangleq \frac{p_F - p_E}{1 - p_E} = \frac{p_F - p_E}{p_E} Odds(p_E) = (p_F/p_E - 1) Odds(p_E)$$

The Heidke skill score scales the odds that the reference model makes a correct prediction by the assessment model's relative change in prediction accuracy. Assessment models earn positive scores—with a maximum possible value of 1—when they are more accurate than the reference model. Similarly, assessment models earn negative scores when they are less accurate than the reference model. Skill scores of 0 indicate the assessment model has the same prediction accuracy as the reference model.

The full disjoint covariate model (1) that incorporates both local covariates and Pacific Ocean sea surface temperatures frequently yields better predictions than either comparison model, which only incorporate local covariates or the remote Pacific Ocean sea surface temperatures, but not both ([Table 2](#)). The full model performs better than chance ($p_F = 1/3$) in almost all cases. While the model that only incorporates local covariates sometimes outperforms the full model, the improvement is typically minimal. [Figure 4](#) compares the prediction accuracy between the full model and the model that only incorporates local covariates. The plot shows that the full model can improve prediction accuracy by up to 5% and suggests improvements may be more likely when winter precipitation is more variable across Florida.

Prediction improvements are realized because the full disjoint covariate model (1) can use the remote Pacific Ocean sea surface temperature information to correct errors made by the local model. Plots of the categorical predictions for the different models are compared in [Figure 5](#). This plot illustrates that while none of the models were near perfect, the full model best balanced local and remote covariate information when making predictions. The local covariates ([Figure 5](#) subplot B) tended to overpredict the amount of precipitation Southern Florida would receive in 1985. Although

Table 2: Heidke skill scores assessing categorical prediction skill in test years for predictions made only using the remote Pacific Ocean sea surface temperatures (HS_R), only using local covariates (HS_L), or using both local and remote covariates (HS_F). The highest skill for each year is highlighted in bold. The overall accuracy for predictions made with both local and remote covariates is also included (p_F). Predictions that use both local and remote covariates are nearly always better than chance ($p_F = 1/3$) and almost always have more skill, or nearly as much skill, as predictions that use less information.

Year	HS_R	HS_L	HS_F	p_F
1983	0.46	0.63	0.62	0.75
1984	-0.20	0.45	0.55	0.70
1985	0.13	0.28	0.28	0.52
1993	0.26	0.34	0.40	0.60
2000	-0.17	0.94	0.90	0.94
2002	0.44	0.05	0.06	0.38
2005	0.14	0.16	0.20	0.47
2007	-0.32	-0.08	-0.19	0.21

the Pacific Ocean sea surface temperatures (Figure 5 subplot C) did not predict many below average precipitation grid cells in Southern Florida, the full model was able to use this information to lessen many of the overpredictions suggested by the local covariates (Figure 5 subplot D).

4. Discussion. The case study demonstrates that the disjoint covariate model (1) can effectively use remote covariates to make better predictions than standard geostatistical models, which only consider local covariates. The model’s hierarchical process formulation additionally has useful interpretations and properties. Our use of the predictive process to create spatially varying coefficients highlights how our use is analogous to compressing covariate data. Additionally, the Kronecker product structure of the remote coefficients’ prior covariance matrix (10) allows the model to estimate teleconnection effects whose impacts vary over similar ranges as regional climate. The residual regression interpretation for the remote coefficients’ posterior distribution (16) also provides theoretical support that this model can recover known teleconnection patterns, like Florida’s teleconnection with tropical sea surface temperatures seen in Figure 3. However, this

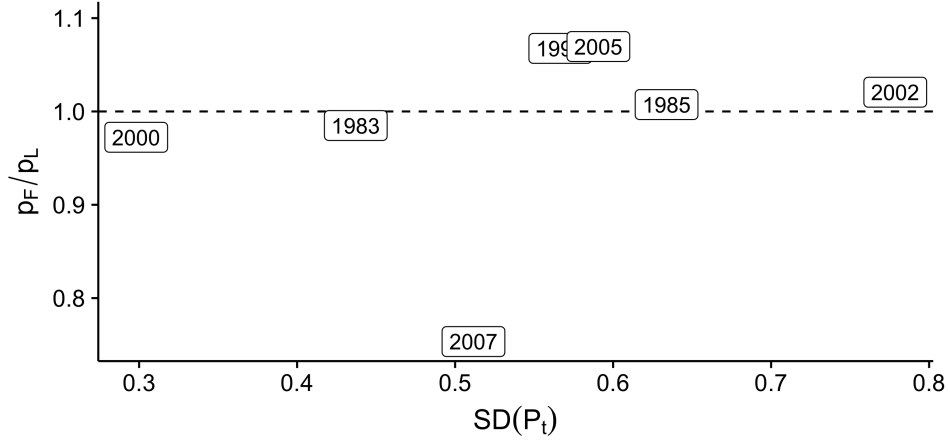


Fig 4: Relative prediction accuracy of categorical predictions made using local covariates and the remote Pacific Ocean sea surface temperatures p_F with respect to categorical predictions made using only local covariates p_L . Relative prediction accuracies are plotted against the Winter standard deviation of precipitation across Florida. Sea surface temperatures can improve prediction accuracy by up to 5% and improvements may be more likely in years with more variability in Winter precipitation.

model may be extended and several open questions remain.

It is uncertain whether categorical predictions should be made by discretizing the posterior predictive distribution or by directly fitting the data to an ordinal model. We anticipate that our choice to discretize the posterior predictive distribution will be most effective since continuous data provides more information than their ordinal summaries, but we have not yet investigated this. We may also consider using probabilistic forecast assessment tools like the probability integral transform described in [Gneiting and Katzfuss \(2014\)](#) to assess model fit instead of using Heidke skill scores. In particular, this could be advantageous since assessments based on the Heidke skill score ignore the ordering of the categorical predictions.

While the disjoint covariate model (1) estimates patterns in the remote coefficients that are consistent with climate science results, the model only finds some statistically significant evidence of individual remote locations within these patterns. Modifying the prior distribution for the remote coefficient parameters or penalizing the likelihood—which can be implemented by appropriate choice of prior distributions (cf. [Park and Casella, 2008](#))—may encourage the disjoint covariate

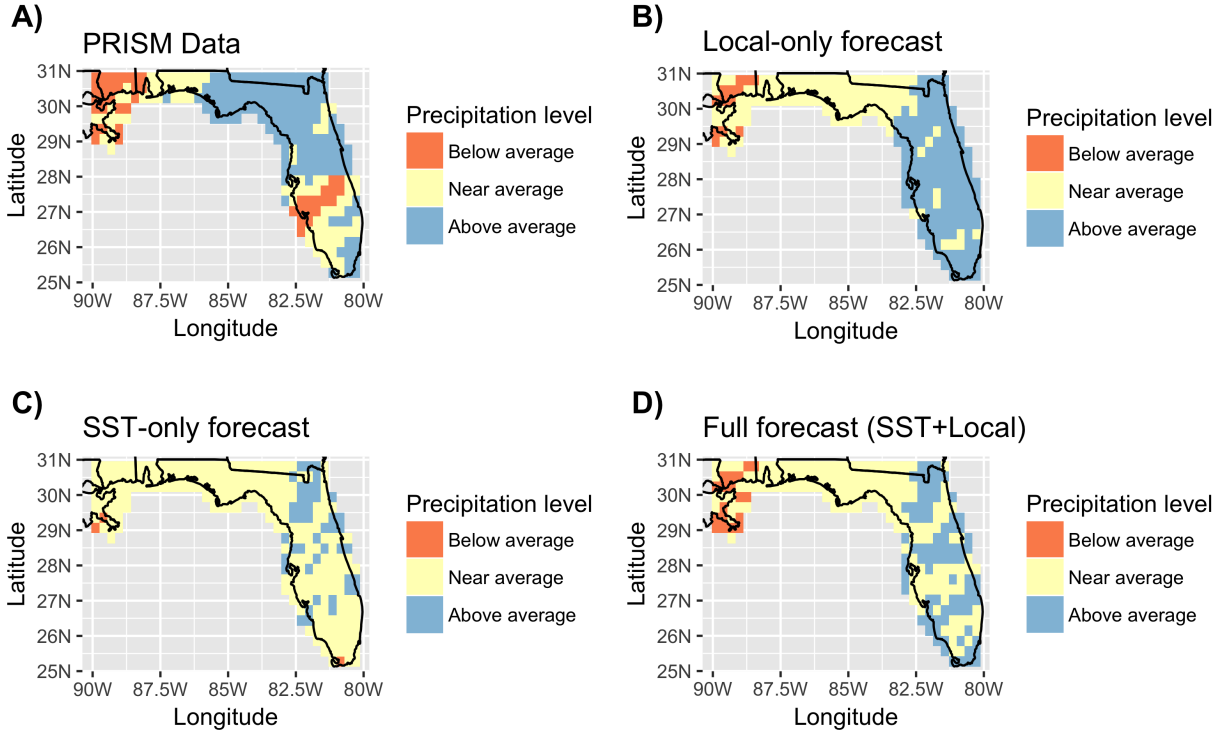


Fig 5: 1985 precipitation level for A) the validation dataset, B) predictions based only on local covariates, C) predictions based only on the remote Pacific Ocean sea surface temperatures (*SST*), and D) predictions based on the full model that uses both local and remote covariates. The results for the full model (D) show it is able to use sea surface temperatures to correct overpredictions in southern Florida from the local-only forecast (B).

model (1) to improve remote coefficient estimates. The significance issue may also be anticipated because the model estimates a large number of random effects. A power study can help further investigate this issue. A simulation study can also further investigate the impact of knot locations on the analysis. Although teleconnection effects are robust, they are also variable (Mason and Goddard, 2001); thus strong statistical significance of remote coefficients may continue to be challenging to detect.

Model fit could potentially be improved by applying more complex spatial models to the local or remote covariates. A nonstationary remote covariance model could, for example, allow the model to estimate different remote coefficient variances and ranges in different parts of the remote domain \mathcal{D}_Z . Allowing the remote coefficients to vary temporally may also improve model fit. The current

model implicitly assumes the teleconnection effects vary slowly enough in time that we may assume they are constant, or that we are estimating their long term average effect. In general, allowing temporally varying remote coefficients risks adopting an unidentifiable model that may overfit the data. This extension, however, may be relevant because [Mason and Goddard \(2001\)](#) find that the effects of remote covariates can vary depending on the overall state of the remote covariate field. As in [Choi et al. \(2015\)](#), these changes may be difficult to detect because the effects tend to be weak. Standard hierarchical geostatistical modeling techniques can also generalize model (1) to include spatially varying coefficients as well as spatio-temporal or nonstationary covariance functions, for example. These generalizations, however, will greatly increase the model's computational demands because the existing model induces a separable covariance structure that makes estimation efficient.

Increased computational demands associated with generalizing model (1) could be offset by applying various approximate spatial modeling techniques to the local or remote covariance matrices. Although we used the predictive process approximation to model the remote coefficients, predictive process approximations can also be applied to the local covariance matrix. Other options include, but are not limited to, Hierarchical Nearest Neighbor models ([Datta et al., 2015](#)), covariance tapering ([Furrer, Genton and Nychka, 2006](#)), and multiresolution covariance models ([Katzfuss, 2016](#)). These techniques could also be used to apply model (1) to higher resolution datasets.

5. Conclusion. We have introduced a geostatistical model that incorporates information from covariates that are spatially disjoint from a spatially correlated response variable. This model addresses a class of spatial analysis problems that standard geostatistical models do not consider. The model applies to spatial analysis problems in which spatial dependence does not follow a central principle in spatial statistics that spatial processes at distant locations are effectively independent. While the model this paper introduces requires that the response and local and remote covariates are defined on disjoint spatial domains, it suggests a broader class of related problems exist in which disjoint domains cannot characterize dependencies between distant locations, or in which appropriate disjoint domains are not known *a priori*, so need to be estimated during model fitting. This problem description is reminiscent of general covariance or graphical model structure estimation problems, suggesting possible directions for future spatial statistics research topics.

The disjoint covariate model (1) also has the potential to move beyond EOF and CCA analyses

to begin working towards grid cell level analyses of teleconnections, and to contribute to timely applications in regional climate and climate impact analyses. Climate change is driving the need for regional planners to predict local climate under future scenarios. This model could help incorporate the combined effects of many teleconnection processes with local covariates to make better predictions. As this model only requires users specify a domain for remote covariates instead of specific teleconnection processes, it could also potentially help improve predictions for areas impacted by unknown teleconnections. The model may also help evaluate teleconnections in global climate models.

Acknowledgements. This material is based upon work supported by the National Science Foundation under Grant Number (NSF AGS - 1419558). Any opinions, findings, and conclusions or recommendations expressed in this material are those of the author(s) and do not necessarily reflect the views of the National Science Foundation.

APPENDIX A: PARTIAL POSTERIOR DISTRIBUTION FOR REMOTE COEFFICIENTS

These computations prove the claim that the marginal posterior distribution (16) for $\boldsymbol{\alpha}^*(\mathbf{s})$ is equivalent to a Bayesian linear regression. The dependence on the g -th posterior sample is excluded from these computations for clarity of presentation.

The full data likelihood (9) yields the marginal data likelihood for a single location $\mathbf{s} \in \mathcal{D}_Y$:

$$\mathbf{Y}(\mathbf{s}) = (Y(\mathbf{s}, t_1) \dots Y(\mathbf{s}, t_{n_t}))^T \Big| \tilde{\boldsymbol{\alpha}}^*, \boldsymbol{\beta}, R^*, \mathbf{c}^*, \Sigma \sim \mathcal{N} \left(\mathbf{X}(\mathbf{s})\boldsymbol{\beta} + \mathbf{Z}^{*T}\boldsymbol{\alpha}^*(\mathbf{s}), \Sigma_{\mathbf{s},\mathbf{s}}I_{n_t} \right)$$

in which $\mathbf{X}(\mathbf{s}) = \left[\mathbf{x}(\mathbf{s}, t)^T \right]_{t=t_1}^{t_{n_t}} \in \mathbb{R}^{n_t \times p}$. The likelihood for the local error $\mathbf{e}(\mathbf{s})$ naturally follows

$$\mathbf{e}(\mathbf{s}) = \mathbf{Y}(\mathbf{s}) - \mathbf{X}(\mathbf{s})\boldsymbol{\beta} \Big| \tilde{\boldsymbol{\alpha}}^*, R^*, \mathbf{c}^*, \Sigma \sim \mathcal{N} \left(\mathbf{Z}^{*T}\boldsymbol{\alpha}^*(\mathbf{s}), \Sigma_{\mathbf{s},\mathbf{s}}I_{n_t} \right)$$

The prior distribution for the remote coefficients (10) implies $\boldsymbol{\alpha}^*(\mathbf{s})$ has the prior distribution

$$\boldsymbol{\alpha}^*(\mathbf{s}) \Big| \Sigma, R^* \sim \mathcal{N}(\mathbf{0}, \Sigma_{\mathbf{s},\mathbf{s}}R^*)$$

Standard Bayesian linear regression results (cf. [Banerjee, Carlin and Gelfand, 2004](#), Example 4.2) yield the posterior distribution for $\boldsymbol{\alpha}^*(\mathbf{s}) \Big| \mathbf{e}(\mathbf{s}), \mathbf{c}^*, R^*, \Sigma$

$$(21) \quad \boldsymbol{\alpha}^*(\mathbf{s}) \Big| \mathbf{e}(\mathbf{s}), \mathbf{c}^*, R^*, \Sigma \sim \mathcal{N} \left(\left(\frac{\mathbf{Z}^* \mathbf{Z}^{*T}}{\Sigma_{\mathbf{s},\mathbf{s}}} + \frac{R^{*-1}}{\Sigma_{\mathbf{s},\mathbf{s}}} \right)^{-1} \frac{\mathbf{Z}^* \mathbf{e}(\mathbf{s})}{\Sigma_{\mathbf{s},\mathbf{s}}}, \left(\frac{\mathbf{Z}^* \mathbf{Z}^{*T}}{\Sigma_{\mathbf{s},\mathbf{s}}} + \frac{R^{*-1}}{\Sigma_{\mathbf{s},\mathbf{s}}} \right)^{-1} \right)$$

The form of the posterior variance in (21) is immediately recognizably equivalent to (18). Manipulating the mean in (21) finishes the claim's proof by showing its form is equivalent to (17):

$$\begin{aligned}
& \left(\frac{\mathbf{Z}^* \mathbf{Z}^{*T}}{\Sigma_{\mathbf{s}, \mathbf{s}}} + \frac{R^{*-1}}{\Sigma_{\mathbf{s}, \mathbf{s}}} \right)^{-1} \frac{\mathbf{Z}^* \mathbf{e}(\mathbf{s})}{\Sigma_{\mathbf{s}, \mathbf{s}}} = \left(\mathbf{Z}^* \mathbf{Z}^{*T} + R^{*-1} \right)^{-1} \mathbf{Z}^* \mathbf{e}(\mathbf{s}) \\
& = \left(\mathbf{Z}^* \mathbf{Z}^{*T} + R^{*-1} \right)^{-1} \begin{bmatrix} \sum_{t \in \mathcal{T}} z^*(\mathbf{r}_1^*, t) (Y(\mathbf{s}, t) - \mathbf{x}(\mathbf{s}, t)^T \boldsymbol{\beta}) \\ \vdots \\ \sum_{t \in \mathcal{T}} z^*(\mathbf{r}_k^*, t) (Y(\mathbf{s}, t) - \mathbf{x}(\mathbf{s}, t)^T \boldsymbol{\beta}) \end{bmatrix} \\
& = \left(\mathbf{Z}^* \mathbf{Z}^{*T} + R^{*-1} \right)^{-1} \sum_{t \in \mathcal{T}} (Y(\mathbf{s}, t) - \mathbf{x}(\mathbf{s}, t)^T \boldsymbol{\beta}) \mathbf{z}_t^*
\end{aligned}$$

APPENDIX B: LOWER BOUND FOR VIFS

Variance inflation factors computed using (19) can attain a minimum value of 1. This can be briefly demonstrated by examining C :

$$C = \left(I_{n_t} + \mathbf{Z}^{*T} R^* \mathbf{Z}^* \right)^{-1}$$

We see $C \rightarrow I_{n_t}$ as $\sigma_\alpha^2 \downarrow 0$ which implies $VIF(\beta_i) \rightarrow 1$. Next, we use the Sherman-Woodbury-Morrison equation to rewrite C :

$$C = I_{n_t} - \mathbf{Z}^{*T} \left(R^{*-1} + \mathbf{Z}^* \mathbf{Z}^{*T} \right)^{-1} \mathbf{Z}^*$$

Properties of positive definite matrices and Kronecker products lets us note that $\left(R^{*-1} + \mathbf{Z}^* \mathbf{Z}^{*T} \right)^{-1}$, and thus $\left(R^{*-1} + \mathbf{Z}^* \mathbf{Z}^{*T} \right)^{-1} \otimes \Sigma^{-1}$ are positive definite matrices. Kronecker product properties further let us see that the remote covariates decrease the posterior precision for β_i relative to spatial regressions without remote coefficients because

$$\mathbf{X}^T (C \otimes \Sigma^{-1}) \mathbf{X} = \mathbf{X}^T (I_{n_t} \otimes \Sigma^{-1}) \mathbf{X} - \mathbf{X}^T \left(\mathbf{Z}^{*T} \otimes I_{n_t} \right) \left(\left(R^{*-1} + \mathbf{Z}^* \mathbf{Z}^{*T} \right)^{-1} \otimes \Sigma^{-1} \right) (\mathbf{Z}^* \otimes I_{n_t}) \mathbf{X}$$

The decreased precision implies the posterior variance for β_i is larger in the disjoint covariate model (1) than in the standard spatial model, which lets us conclude $VIF(\beta_i) \geq 1$. A more detailed argument can suggest the variance inflation factors are also bounded from above by a constant that depends on the data.

REFERENCES

ANDRIEU, C. and THOMS, J. (2008). A tutorial on adaptive MCMC. *Statistics and Computing* **18** 343–373.

ASHOK, K., BEHERA, S. K., RAO, S. A., WENG, H. and YAMAGATA, T. (2007). El Niño Modoki and its possible teleconnection. *Journal of Geophysical Research* **112** 1–27.

BANERJEE, S., CARLIN, B. P. and GELFAND, A. E. (2004). *Hierarchical Modeling and Analysis for Spatial Data*, 1 ed. Chapman and Hall/CRC, Boca Raton, FL.

BANERJEE, S., GELFAND, A. E., FINLEY, A. O. and SANG, H. (2008). Gaussian predictive process models for large spatial data sets. *Journal of the Royal Statistical Society. Series B: Statistical Methodology* **70** 825–848.

CHOI, I., LI, B., ZHANG, H. and LI, Y. (2015). Modelling space-time varying ENSO teleconnections to droughts in North America. *Stat* **4** 140–156.

DALY, C., HALBLEIB, M., SMITH, J. I., GIBSON, W. P., DOGGETT, M. K., TAYLOR, G. H., CURTIS, J. and PASTERIS, P. P. (2008). Physiographically sensitive mapping of climatological temperature and precipitation across the conterminous United States. *International Journal of Climatology*.

DATTA, A., BANERJEE, S., FINLEY, A. and GELFAND, A. (2015). Hierarchical Nearest-Neighbor Gaussian Process Models for Large Geostatistical Datasets. *Journal of the American Statistical Association* **June**.

DEE, D. P., UPPALA, S. M., SIMMONS, A. J., BERRISFORD, P., POLI, P., KOBAYASHI, S., ANDRAE, U., BALMASEDA, M. A., BALSAMO, G., BAUER, P., BECHTOLD, P., BELJAARS, A. C. M., VAN DE BERG, L., BIDLOT, J., BORMANN, N., DELSOL, C., DRAGANI, R., FUENTES, M., GEER, A. J., HAIMBERGER, L., HEALY, S. B., HERSBACH, H., HÓLM, E. V., ISAKSEN, L., KÅLLBERG, P., KÖHLER, M., MATRICARDI, M., McNALLY, A. P., MONGESANZ, B. M., MORCRETTE, J. J., PARK, B. K., PEUBEY, C., DE ROSNAY, P., TAVOLATO, C., THÉPAUT, J. N. and VITART, F. (2011). The ERA-Interim reanalysis: Configuration and performance of the data assimilation system. *Quarterly Journal of the Royal Meteorological Society* **137** 553–597.

DOUGLAS, A. V. and ENGLEHART, P. J. (1981). On a Statistical Relationship between Autumn Rainfall in the Central Equatorial Pacific and Subsequent Winter Precipitation in Florida. *Monthly Weather Review* **109** 2377–2382.

FURRER, R., GENTON, M. G. and NYCHKA, D. (2006). Covariance Tapering for Interpolation of Large Spatial Datasets. *Journal of Computational and Graphical Statistics* **15** 502–523.

GNEITING, T. and KATZFUSS, M. (2014). Probabilistic Forecasting. *Annual Review of Statistics and Its Application* **1** 125–151.

HOTELLING, H. (1936). Relations Between Two Sets of Variates. *Biometrika* **28** 321–377.

KATZFUSS, M. (2016). A multi-resolution approximation for massive spatial datasets. *Journal of the American Statistical Association*.

MANTUA, N. J., HARE, S. R., ZHANG, Y., WALLACE, J. M. and FRANCIS, R. C. (1997). A Pacific Interdecadal Climate Oscillation with Impacts on Salmon Production. *Bulletin of the American Meteorological Society* **78** 1069–1079.

MASON, S. J. and GODDARD, L. (2001). Probabilistic precipitation anomalies associated with ENSO. *Bulletin of the American Meteorological Society* **82** 619–638.

MISRA, V. and DINAPOLI, S. M. (2013). Understanding the wet season variations over Florida. *Climate Dynamics* **40** 1361–1372.

MO, K. C. (2003). Ensemble canonical correlation prediction of surface temperature over the United States. *Journal*

of climate **16** 1665–1683.

PARK, T. and CASELLA, G. (2008). The Bayesian Lasso. *Journal of the American Statistical Association* **103** 681–686.

PARKER, D. J. (2015). Mesoscale Meteorology. *Encyclopedia of Atmospheric Sciences* 316–322.

PÉBAY, P. (2008). Formulas for Robust, One-Pass Parallel Computation of Covariances and Arbitrary-Order Statistical Moments. *Sandia Report September*.

REICH, B. J., HODGES, J. S. and ZADNIK, V. (2006). Effects of residual smoothing on the posterior of the fixed effects in disease-mapping models. *Biometrics* **62** 1197–1206.

TOWLER, E., PAIMAZUMDER, D. and HOLLAND, G. (2016). A framework for investigating large-scale patterns as an alternative to precipitation for downscaling to local drought. *Climate Dynamics* 1–12.

TRENBERTH, K. E. (1997). The Definition of El Nino. *Bulletin of the American Meteorological Society* **78** 2771–2777.

VON STORCH, H. and ZWIERS, F. W. (1999). *Statistical Analysis in Climate Research*. Cambridge University Press, Cambridge.